Journal of Electronic Research and Application, 2026, Volume 10, Issue 6
http://ojs.bbwpublisher.com/index.php/JERA
Online ISSN: 2208-3510
Print ISSN: 2208-3502

Design and Simulation of a Miniaturized Printed Wideband Antenna with a Gradual Radiator and Defected Ground

Qi Wang

School of Electronic and Information Engineering, Liaoning Technical University (Huludao Campus), Huludao 125105, Liaoning Province, China

***Corresponding author:** Qi Wang,wangqi545@163.com

Abstract: To improve the integration capability and impedance matching of printed antennas for wideband wireless terminals, a miniaturized planar antenna with a gradual radiator and a defected partial ground is designed and verified by full-wave simulation. The antenna is implemented on an FR4 substrate of 31 mm × 18 mm × 1 mm and fed by a 50 Ohm microstrip line. A gradual, chamfered radiator with a top arc and T-shaped loading is combined with a partial ground containing a central slot and tapered edge, so that the forward and return current paths can be tuned simultaneously. The Driven Modal solver in Ansys HFSS is used to evaluate the reflection coefficient, field, and current distributions, and far-field radiation. The simulated S11 curve exhibits resonances near 3.3 GHz, 4.4–4.6 GHz, 7.7–8.0 GHz, and 13.0 GHz; the deepest resonance reaches about -35 dB, and the typical peak GainTotal is about 3.2 dBi. A parameter sweep of La from 0.6 mm to 0.8 mm shows little influence on the main resonances. The results indicate that the proposed structure provides a compact and feasible basis for multi-band or wideband terminal antennas.

Keywords: Printed antenna; Ultra-wideband antenna; Defected ground structure; HFSS; Impedance matching

Online publication: Jul 7, 2026

1. Introduction

Antennas are key interfaces in wireless communication and electromagnetic sensing systems because they convert guided waves in circuits into radiated waves in free space. Their impedance matching, bandwidth, and radiation characteristics directly influence link budget, coverage, and system integration. With the continuous miniaturization of terminals, a compact antenna must maintain acceptable matching and stable radiation within a limited printed-circuit-board area [1,2].

Printed planar antennas, including microstrip-fed monopole and slot-loaded forms, are widely adopted because of their low profile, low cost, and compatibility with standard PCB processes [3]. However, their

resonant behavior is highly sensitive to the geometry of the radiator, feeding transition, ground plane, and slot defects [4]. Small changes in these structures may alter the surface-current path, shift resonant points, and introduce multi-mode coupling [5]. Therefore, full-wave modeling and targeted parameter optimization are essential in practical design [6].

Ultra-wideband (UWB) applications require an antenna to maintain good impedance matching over a broad spectral range while remaining tolerant of narrowband interference [7,8]. Reported solutions usually employ gradual radiators, loaded branches, slots, and defective ground structures (DGS) to form multiple resonances or controllable notched bands [9]. Based on this design concept, this paper presents a miniaturized printed wideband antenna and analyzes its matching and radiation mechanisms by HFSS simulation [10].

2. Antenna structure and simulation method

2.1. Antenna configuration

The proposed antenna adopts a double-sided printed structure on an FR4 substrate. The overall size is 31 mm x 18 mm x 1 mm, which is suitable for compact terminal integration. The top layer contains a gradual and chamfered radiator connected to a 50 Ohm microstrip feed. A top arc and T-shaped loading are introduced to extend the effective current path and to generate additional resonant modes. The bottom layer uses a partial ground plane with a central slot and tapered upper edge, which modifies the return-current path and equivalent capacitance/inductance, thereby improving impedance transition over a wider frequency range. See **Figure 1** and **Table 1**.

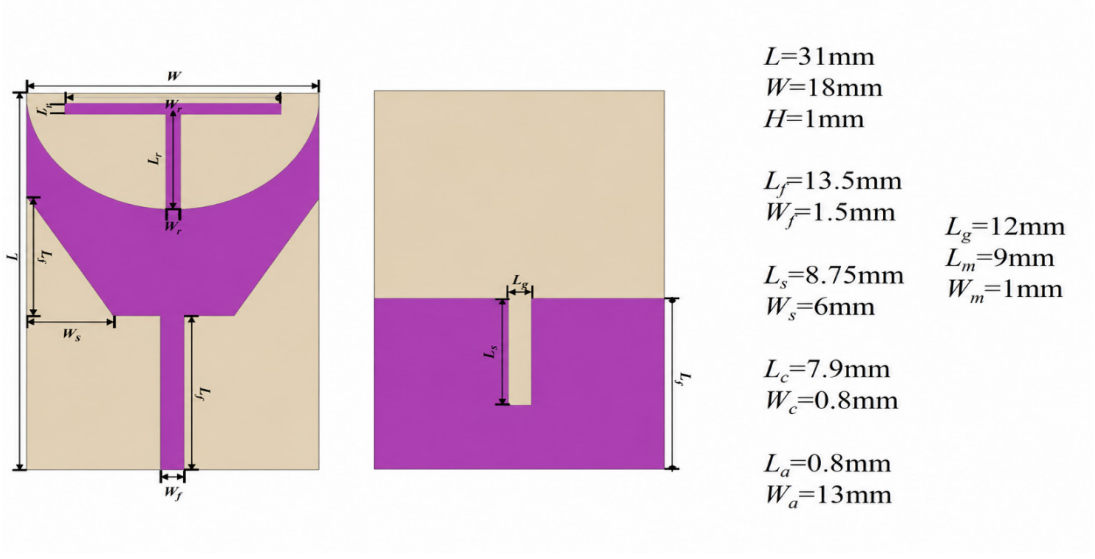

Figure 1. Geometry and main dimensions of the miniaturized printed antenna.

Table 1. Main design parameters and simulated performance indicators

Category	Parameter or output	Value / description
Substrate	Material and size	FR4, 31 mm × 18 mm × 1 mm
Feeding	Reference impedance	50 Ohm microstrip feed
Radiator	Geometry tuning	Gradual/chamfered radiator with top arc and T-shaped loading

Ground	DGS treatment	Partial ground with tapered edge and central slot
Solver	Simulation platform	Ansys HFSS, Driven Modal frequency-domain analysis
Matching	Main resonances	3.3, 4.4–4.6, 7.7–8.0, and 13.0 GHz
Radiation	Typical peak GainTotal	About 3.2 dBi at the selected operating frequency
Sensitivity	La sweep	0.6–0.8 mm with 0.05 mm step; main response nearly unchanged

2.2. Simulation setup

The model is built in Ansys HFSS with parameterized substrate, radiator, feed, and ground features. The Driven Modal solution is employed for frequency-domain analysis, and a radiation air box is assigned around the antenna. The reflection coefficient S11 is used as the primary matching index, and S11 ≤ -10 dB is adopted as the engineering criterion for a usable operating band. The initial electrical size is estimated from a quarter-wavelength current-path assumption, while final resonance positions are determined by full-wave simulation because the actual current flows along the radiator edge, loading branch, and ground-return path.

3. Simulation results and discussion

3.1. Impedance matching characteristics

The simulated S11 response shows a clear multi-resonant behavior, as shown in Figure 2. The deepest resonance occurs near 3.3 GHz with a return loss of about -35 dB, indicating excellent impedance matching around the lowest operating mode. Additional resonant dips appear near 4.4–4.6 GHz, 7.7–8.0 GHz, and 13.0 GHz, with approximate return-loss levels of -25 dB, -20 dB, and -15 dB, respectively. These dips confirm that the combined radiator loading and defective ground introduce several effective current paths rather than a single narrow-band resonance. See **Figure 2**.

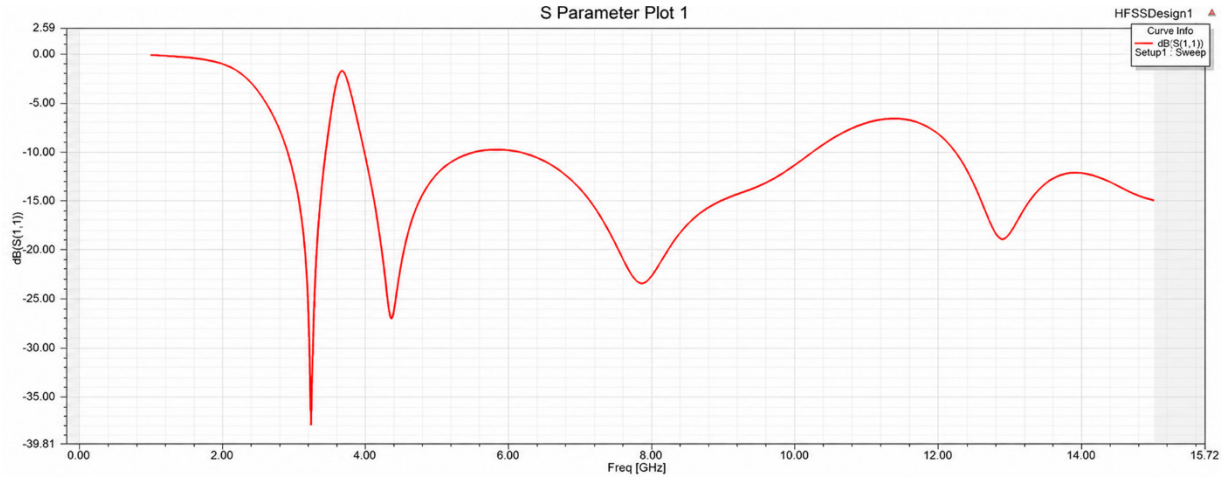

Figure 2. Simulated S11 curve of the proposed antenna.

A further sweep of parameter La from 0.6 mm to 0.8 mm with a step of 0.05 mm indicates that the main resonant positions and depths are almost unchanged. This result suggests that La is not the dominant tuning parameter in the present configuration. In contrast, the low-frequency resonance is expected to be more strongly associated with the total path length from the feed to the radiator edge and the ground return,

whereas higher-frequency modes are more sensitive to the local top-loading, slot, and DGS features.

3.2. Radiation behavior and mechanism

Far-field post-processing yields a typical peak GainTotal of about 3.2 dBi, and the two-dimensional E-plane/H-plane patterns show that the antenna exhibits identifiable main radiation regions. Although the design is not intended for high-gain directional operation, the positive gain indicates that the matched input power can be effectively radiated into free space. Surface-current and electric-field distributions further show that strong current appears along the microstrip feed, the feed-radiator transition, and the upper loading region. This concentration is consistent with the edge-radiation mechanism of printed planar antennas.

The multi-resonant response can therefore be interpreted from the coexistence of several current paths. The low-frequency mode is mainly governed by the global path consisting of feed, radiator, and ground return, while the middle and high-frequency modes are produced by local loading and slot perturbations. The present structure provides a compact platform for multi-band operation; however, if a continuous UWB passband or explicit notched-band suppression is required, the radiator loading, ground-slot length, and slot position should be optimized more systematically.

3.3. Mode attribution and parameter sensitivity

To further clarify the electromagnetic mechanism, the simulated resonances can be associated with different equivalent current paths rather than treated only as isolated numerical dips. The resonance near 3.3 GHz is primarily determined by the global path from the microstrip feed to the gradual radiator edge and then to the ground return. This mode is responsible for the lowest usable band and is therefore strongly related to the overall electrical length of the printed structure. The 4.4–4.6 GHz resonance is influenced by the feed-radiator transition and the upper arc, which introduce a smoother impedance transition and additional capacitive coupling. The 7.7–8.0 GHz and 13.0 GHz responses are more closely associated with local perturbations caused by the T-shaped loading, central ground slot and tapered ground edge.

The parameter sweep of La from 0.6 mm to 0.8 mm, with a step of 0.05 mm, shows that the major resonant positions and return-loss depths remain nearly unchanged. This indicates that La is not the primary control variable in the present geometry and that the antenna response has a certain tolerance to small dimensional variations of this parameter. From an engineering perspective, such robustness is useful in PCB fabrication because small etching deviations or alignment errors are unlikely to disrupt the main matching behavior. By contrast, parameters directly related to the total current path, such as the length of the top loading strip, the gap between the radiator and the partial ground, and the length and width of the ground slot, are expected to have a stronger influence on impedance matching and should be emphasized in subsequent optimization. See **Table 2**.

Table 2. Physical interpretation of the simulated resonant modes

Mode	Frequency range	Dominant structural factor	Design implication
M1	about 3.3 GHz	Global feed-radiator-ground current path	Sets the lowest operating mode and compact-size limit
M2	4.4–4.6 GHz	Feed transition and top arc coupling	Improves local matching after the first resonance
M3	7.7–8.0 GHz	T-shaped loading and slot perturbation	Provides an additional middle/high-frequency matching point

M4	about 13.0 GHz	Higher-order edge and DGS current path	Extends usable matching tendency to the high-frequency range

3.4. Optimization strategy and engineering applicability

Although the proposed antenna achieves compact multi-resonant matching, the S11 response still does not form a fully continuous UWB passband. Adjacent resonances can be merged by jointly tuning the radiator contour, ground-slot length and position, microstrip transition width, and feed-region coupling. For practical implementation, FR4 loss, copper thickness, SMA connector, soldering pad, and finite-ground effects may reduce gain or shift the input impedance; therefore, prototype fabrication and vector-network-analyzer measurements are necessary for final validation. Overall, the workflow of current-path estimation, HFSS simulation, and field/current analysis is repeatable and can support future bandwidth extension, notch-band design, and radiation-stability optimization.

4. Conclusion

A compact printed wideband antenna based on a gradual radiator and a defected partial ground has been designed and simulated. The antenna occupies only 31 mm × 18 mm × 1 mm on an FR4 substrate and is excited by a 50 Ohm microstrip feed. HFSS results show resonant points near 3.3 GHz, 4.4–4.6 GHz, 7.7–8.0 GHz, and 13.0 GHz, with the best simulated return loss reaching about -35 dB. The typical peak GainTotal is about 3.2 dBi, and the current distribution verifies that the feed transition, radiator edge, and top loading form the main radiation and tuning regions. The study demonstrates that simultaneous control of the forward current path and ground-return path is effective for compact multi-band matching. Future work should focus on merging adjacent resonances to obtain a more continuous UWB passband and on introducing controllable notch structures for interference suppression.

Disclosure statement

The author declares no conflict of interest.

References

[1] Xiang L, Wei K, Zhang X, et al., 2025, A Miniaturized and Wideband Millimeter-Wave ± 45° Differentially Fed Dual-Polarized Arrowhead-Shaped Patch Antenna Array. IEEE Antennas and Wireless Propagation Letters, 24(12): 4760–4764.

[2] Wang B, Zhou Z, Deng C, et al., 2025, A Compact D-Band Multilayer Horn Antenna with Thin 3-D-Printed Lens for Subterahertz Applications. IEEE Antennas and Wireless Propagation Letters, 24(9): 2919–2923.

[3] Zhou X, Zhang G, Tam K, et al., 2026, Folded-Patch-Based Miniaturized Quasi-Omnidirectional Filtering Antennas. IEEE Transactions on Antennas and Propagation, 74(1): 298–308.

[4] Kumar P, Rao P, Saxena S, 2025, Design and Analysis of 0.5–2.0 GHz RF Frontend Subsystems for IEMI Applications. IEEE Transactions on Electromagnetic Compatibility, 67(1): 237–246.

[5] Mazzinghi A, Barras D, Danev B, et al., 2024, Miniaturized UWB Dual-Port Antenna for Localization Applications. IEEE Antennas and Wireless Propagation Letters, 23(3): 1080–1084.

[6] Salimitorkamani M, Mehranpour M, Odabasi H, 2024, A Miniaturized Wideband Sinuous Antenna for Microwave Brain Imaging Systems. IEEE Transactions on Antennas and Propagation, 72(3): 2228–2240.

[7] Shukoor M, Dey S, 2024, Wideband Reconfigurable Multifunctional Absorber/Reflector with Bandpass/Bandstop Filtering and Band-Notch Absorption for RCS and EMI Shielding. IEEE Transactions on Electromagnetic Compatibility, 66(1): 153–160.

[8] Askarzadeh R, Farahbakhsh A, Zarifi D, et al., 2025, Wideband High-Efficiency Slot Array Antenna Based on Gap Waveguide Single-Layer Feeding Network. IEEE Antennas and Wireless Propagation Letters, 24(2): 519–523.

[9] Li D, Deng C, Fu Z, et al., 2025, Wideband Electrically Small Vivaldi Antenna Using Non-Foster Matching. IEEE Antennas and Wireless Propagation Letters, 24(8): 2672–2676.

[10] Cheng S, Chen S, Huang W, 2025, Low-Profile MIMO Trapezoidal Patch Antenna for 5G Wideband Mobile Antenna Application. IEEE Antennas and Wireless Propagation Letters, 24(3): 696–700.